Physics of the Dark Universe 37 (2022) 101063

Contents lists available at ScienceDirect

Physics of the Dark Universe

journal homepage: www.elsevier.com/locate/dark

Using neutrino oscillations to measure H_0

Ali Rida Khalifeh [a,b,*], Raul Jimenez [a,c]

[a] ICC, University of Barcelona, Marti i Franques, 1, E-08028 Barcelona, Spain
[b] Dept. de Fisica Cuantica y Astrofisica, University of Barcelona, Marti i Franques 1, E-08028 Barcelona, Spain
[c] ICREA, Pg. Lluis Companys 23, Barcelona, E-08010, Spain

ARTICLE INFO

Article history:
Received 19 December 2021
Received in revised form 28 April 2022
Accepted 30 May 2022

Keywords:
Quantum field theory in curved spacetime
Neutrino oscillations
Hubble tension

ABSTRACT

The tension between late and early universe probes of today's expansion rate, the Hubble parameter H_0, remains a challenge for the standard model of cosmology ΛCDM. There are many theoretical proposals to remove the tension, with work still needed on that front. However, by looking at new probes of the H_0 parameter one can get new insights that might ease the tension. Here, we argue that neutrino oscillations could be such a probe. We expand on previous work and study the full three-flavor neutrino oscillations within the ΛCDM paradigm. We show how the oscillation probabilities evolve differently with redshift for different values of H_0 and neutrino mass hierarchies. We also point out how this affects neutrino fluxes which, from their measurements at neutrino telescopes, would determine which value of H_0 is probed by this technique, thus establishing the aforementioned aim.

1. Introduction

The Hubble tension, the discrepancy between early and late universe measurements of the Hubble parameter H_0, is still persisting [1,2]. Early universe probes are mainly from Cosmic Microwave Background (CMB) experiments, such as the ones from [3,4]. This parameter is determined assuming Λ Cold Dark Matter (ΛCDM) as the fiducial cosmological model, combined with measurements independent from it. On the other hand, late universe measurements use the local distance ladder method [5,6] on Cepheids, type-Ia supernovae and tip of the red giant branch in a way independent from the cosmological model [7,8].

To solve this tension, several theoretical models have been proposed, including early dark energy [9,10] and modified gravity [11] (see [12] for a recent and thorough review on the subject). However, one can gain new insight on this tension by developing new observables, being late or early universe ones, that are affected by today's expansion rate.

In this work, we build on previous ones [13,14] and show the possibility of using neutrino oscillations as a new probe for the Hubble tension. Although the latter has been looked at in connection with neutrinos previously [15], our approach is quite different. We consider a system of three-flavor neutrinos, $(\nu_e, \nu_\mu, \nu_\tau)$, traveling in a flat Friedmann–Lemaître–Robertson–Walker (FRW) spacetime with a cosmological constant Dark energy (DE) Λ. By studying the transition probabilities' evolution from one flavor to another as a function of redshift, we show how different values of H_0 affect the detected neutrino fluxes, making the latter a potential probe for H_0. In our analysis, we consider different initial conditions (ICs) for neutrino flavor composition, and distinguish between their mass hierarchies.

It should be noted that there have been a great deal of work in the literature done on neutrinos as spinors in curved spacetime. We direct the interested reader to a few of them and references therein [16–26].

The organization of the paper is as follows: we briefly present the necessary principles and equations for the analysis in Section 2. Then, we present and discuss the main results, given as triangular plots, what is called ternary diagrams, and fluxes' evolution with redshift, in Section 3. Current and future observational prospects are discussed in Section 4, before finishing with some concluding remarks in Section 5.

We use units in which $\hbar = c = 1$ and a metric signature $(-,+,+,+)$. Moreover, data from [3] is used to get an early universe (EU) value of H_0, what we call $H_0^{EU} = 2.13\times10^{-33}h^{\rm EU}$ eV, where $h^{\rm EU} = 0.674$. In addition to that, matter and DE density parameters $\Omega_{m(\Lambda)} = 8\pi G/(3H_0^2)\rho_{m(\Lambda)}$, where ρ_m, ρ_Λ are the energy densities of matter and DE, respectively, are also taken from [3]. For the late universe (LU) value of H_0, H_0^{LU}, we use results from [27], which gives $H_0^{LU} = 2.13\times10^{-33}h^{\rm LU}$ eV, with $h^{\rm LU} = 0.740$.

Notation wise, neutrino flavor states will be denoted by Greek indices, while Latin ones denote mass eigenstates.

* Corresponding author at: ICC, University of Barcelona, Marti i Franques, 1, E-08028 Barcelona, Spain.
E-mail addresses: ark93@icc.ub.edu (A.R. Khalifeh), raul.jimenez@icc.ub.edu (R. Jimenez).

https://doi.org/10.1016/j.dark.2022.101063

2. Neutrinos in flat FLRW universe

In this section, we will follow a practical approach in which we briefly describe the relevant equations and principles needed for the case under study. We refer the unfamiliar reader to [13,14] and references therein for a more thorough derivation.

In the concordance ΛCDM model, spacetime is best described by a flat FLRW metric $g_{\mu\nu}$, given by the line element

$$ds^2 = g_{\mu\nu}dx^\mu dx^\nu = -dt^2 + a^2(t)\left(dr^2 + r^2 d\theta^2 + r^2\sin^2\theta d\phi^2\right) \quad (1)$$

in terms of cosmic time t and spherical coordinates $\{r, \theta, \phi\}$. Moreover, $a(t)$, the scale factor, is independent of spatial coordinates due to homogeneity and isotropy of FRW. Following the usual machinery in Cosmology [28,29], one gets the first Friedmann equation

$$H^2(z) = \frac{8\pi G}{3}\left(\rho_m + \rho_\Lambda\right) = H_0^2\left(\Omega_m(1+z)^3 + \Omega_\Lambda\right) \quad (2)$$

where $z = a_0/a - 1$ is the redshift, with a_0 being today's value of $a(t)$.

This is what we will be needing from the gravity side. On the neutrino part, to study their oscillations in curved spacetime, we are mainly interested in the transition amplitude between two flavor states $|\nu_\alpha\rangle$ and $|\nu_\beta\rangle$, $\Psi_{\alpha\beta}$, from which we get the oscillation probability $P_{\alpha\beta}$:

$$\Psi_{\alpha\beta} \equiv \langle\nu_\beta|\nu_\alpha\rangle \Rightarrow P_{\alpha\beta} = |\Psi_{\alpha\beta}|^2. \quad (3)$$

As was shown previously [14], $\Psi_{\alpha\beta}$ evolves with the affine parameter λ for the case of ΛCDM as:

$$i\frac{d}{d\lambda}\Psi_{\alpha\beta} = \frac{1}{2}\mathcal{M}_f^2\Psi_{\alpha\beta}, \quad (4)$$

where

$$\mathcal{M}_f^2 = U\begin{pmatrix} m_1^2 & 0 & 0 \\ 0 & m_2^2 & 0 \\ 0 & 0 & m_3^2 \end{pmatrix}U^\dagger \quad (5)$$

is the square of the vacuum mass matrix in flavor space. In the above equation, m_i, for $i = 1, 2, 3$, are the eigenvalues of the neutrino mass states, $|\nu_i\rangle$, and $U_{\alpha j}$ is the Pontecorvo–Maki–Nakagawa–Sakata(PMNS) matrix for neutrino mixing [30,31], with the $\dagger$ corresponding to Hermitian conjugation. More explicitly, the latter can be written in terms of mixing angles θ_{ij}, for $\{i, j\} = 1, 2, 3$, as [32]

$$U = \begin{pmatrix} c_{12}c_{13} & s_{12}c_{13} & s_{13}e^{-i\delta} \\ -s_{12}c_{23} - s_{13}s_{23}c_{12}e^{i\delta} & c_{12}c_{23} - s_{12}s_{23}s_{13}e^{i\delta} & s_{23}c_{13} \\ s_{12}s_{23} - s_{13}c_{12}c_{23}e^{i\delta} & -s_{23}c_{12} - s_{12}s_{13}c_{23}e^{i\delta} & c_{13}c_{23} \end{pmatrix} \quad (6)$$

where $c_{ij} \equiv \cos\theta_{ij}$, $s_{ij} \equiv \sin\theta_{ij}$ and δ is the Charge Conjugation-Parity (CP) violating phase. Incidentally, here we are considering neutrinos to be of the Dirac type, hence there is one CP violating phase (see [33,34] for a review on CP violation and the nature of neutrinos).

If we start with an initial state $|\nu_\alpha\rangle$, then Eq. (4) can be written explicitly as

$$i\frac{d}{d\lambda}\begin{pmatrix}\Psi_{\alpha e}\\ \Psi_{\alpha\mu}\\ \Psi_{\alpha\tau}\end{pmatrix} = \frac{1}{2}U\begin{pmatrix} m_1^2 & 0 & 0 \\ 0 & m_2^2 & 0 \\ 0 & 0 & m_3^2 \end{pmatrix}U^\dagger\begin{pmatrix}\Psi_{\alpha e}\\ \Psi_{\alpha\mu}\\ \Psi_{\alpha\tau}\end{pmatrix} \quad (7)$$

for the transition of α to any of the three flavors e, μ and τ. By defining

$$\Phi_\alpha \equiv U^\dagger\Psi_\alpha, \quad (8)$$

Eq. (7) becomes, after multiplying it with $U^\dagger$ from the left,

$$i\frac{d}{d\lambda}\begin{pmatrix}\Phi_{\alpha 1}\\ \Phi_{\alpha 2}\\ \Phi_{\alpha 3}\end{pmatrix} = \frac{1}{2}\begin{pmatrix} m_1^2 & 0 & 0 \\ 0 & m_2^2 & 0 \\ 0 & 0 & m_3^2 \end{pmatrix}\begin{pmatrix}\Phi_{\alpha 1}\\ \Phi_{\alpha 2}\\ \Phi_{\alpha 3}\end{pmatrix}. \quad (9)$$

Here, we have used the unitarity condition of the PMNS, $U^\dagger U = I$, where I is the 3×3 identity matrix. As one can see, by going from Eq. (7) to Eq. (9) we have simply changed from flavor to mass basis. This will make it easier to solve the evolution equation, and then we can simply transform back to the flavor basis by the inverse of (8).

The solution to each $\Phi_{\alpha j}$ is

$$\Phi_{\alpha j}(\lambda) = \Phi_\alpha^{\rm ini}e^{-i\frac{1}{2}m_j^2\Delta\lambda} \quad (10)$$

where $\Phi_\alpha^{\rm ini}$ is the initial neutrino composition at emission in mass basis, and [14]

$$\Delta\lambda \equiv \frac{1}{E_0}\int_0^{z_e}\frac{dz}{H(z)(1+z)^2}, \quad (11)$$

with E_0 being the detected neutrino energy on Earth (corresponding to $z = 0$), z_e is the source's redshift and $H(z)$ is given in Eq. (2).

Finally, to get the probability $P_{\alpha\beta}$, there are three steps that need to be done. First, starting from an initial neutrino flavor composition, $\Psi^{\rm ini}$, we apply eq (8) to get $\Phi_\alpha^{\rm ini}$. Second, we plug the latter in the solution Eq. (10) and apply the inverse of Eq. (8) to get the evolution of $\Psi_{\alpha\beta}$. Third, we take the modulus square of that to get an expression for the $\alpha\to\beta$ transition probability of the form:

$$P_{\alpha\beta} = \delta_{\alpha\beta} + \sum_{i<j}\left[a_{\alpha\beta;ij}\sin^2\left(\frac{\Delta m_{ij}^2\Delta\lambda}{4}\right) + b_{\alpha\beta;ij}\sin\left(\frac{\Delta m_{ij}^2\Delta\lambda}{2}\right)\right] \quad (12)$$

where $\delta_{\alpha\beta}$ is the Kronecker delta, $\Delta m_{ij}^2 \equiv m_i^2 - m_j^2$, and the $a_{\alpha\beta;ij}$s[1] and $b_{\alpha\beta;ij}$s are numerical factors resulting from different combinations of PMNS components. In particular, this combination depends on which states α and β are being considered (see eq. (13.9) in [35] for the equivalent form in Minkowski spacetime).

From here, we can apply the above machinery to several initial conditions and see how it affects the probability's evolution with redshift, in addition to that of the flux, which will be the subject of the next section.

3. Observational results for different initial conditions

The space of initial conditions (ICs) for neutrino oscillations, i.e. initial decomposition, has many elements. However, there are three that are more relevant observationally: Neutron decay (ND), Muon damping (MD) and Pion decay (PD). In the representation $(\nu_e : \nu_\mu : \nu_\tau)$ for the initial ratios, these three conditions correspond to $(1:0:0)$, $(0:1:0)$ and $(1/3:2/3:0)$, respectively. In terms of $\Psi_\alpha^{\rm ini}$, this corresponds to

$$\Psi_{\rm ND}^{\rm ini} = \begin{pmatrix}1\\0\\0\end{pmatrix}, \quad \Psi_{\rm MD}^{\rm ini} = \begin{pmatrix}0\\1\\0\end{pmatrix}, \quad \Psi_{\rm PD}^{\rm ini} = \begin{pmatrix}\frac{1}{\sqrt{5}}\\ \frac{2}{\sqrt{5}}\\ 0\end{pmatrix}, \quad (13)$$

normalized such that the sum of probabilities is 1.

Our purpose in this section is to see observational differences between $H_0^{\rm EU}$ and $H_0^{\rm LU}$ in neutrino oscillations. In addition to that, we distinguish between inverted hierarchy (IH) for neutrinos

[1] To avoid confusion, we note that the semicolon does not correspond to any kind of derivative, but it is used just to separate flavor from mass indices.

masses, as well as the normal one (NH). This will result in a total of four cases for each initial neutrino composition Eq. (13): NH-EU, NH-LU, IH-EU and IH-LU. For instance, NH-EU corresponds to having neutrinos in the NH with today's rate of acceleration given by $H_0^{\rm EU}$. In Table 1, we list the values of the different neutrino parameters for both hierarchies as reported in [32].

One thing we can look at observationally is flavor ternary plots. These are triangular diagrams, with each side indicating the percentage of neutrinos from a certain flavor detected. In other words, each side corresponds to the probability of detecting neutrinos with certain flavor, with the sum being always equal to 1. These are shown in Fig. 1, where the first, second and third rows correspond to ND, MD and PD initial conditions, respectively. Moreover, the left side diagrams correspond to NH, while the right side ones to IH. In each diagram, different colors represent the indicated redshifts of emission, diamonds correspond to using $H_0^{\rm EU}$ in the previous section's analysis, while stars correspond to using $H_0^{\rm LU}$. We also include in each diagram the latest IceCube [36] 68% and 95% Confidence Levels (CLs) (see figure 5 of [37]). In addition, for the MD case, we include the 68%(dashed orange) and 95%(dashed blue)CLs expected from IceCube-Gen2, while for the PD case, we show expectations for 68%CLs from 15 years of IceCube Data (dark blue contour) and that combined with 10 years of IceCube-Gen2(yellow contour) [37]. We will discuss more about these forecasts in Section 4.

The first thing to note when looking at these diagrams is the difference between the left and right side ones for each IC. There is a slight distinction between hierarchies throughout their evolution with redshift. Therefore there is no degeneracy between NH and IH as neutrinos travel in an expanding universe, as expected. Second, one can notice an appreciable difference in evolution between different ICs, and therefore we see no degeneracy between them as well. Third, in every diagram, the distinction between EU and LU starts to become appreciable at around $z_e \sim 0.2$.[2] To give a concrete example on this distinction, let us look at the middle-right diagram of Fig. 1 particularly the points corresponding to z = 2. If at some point we detect at neutrino observatories neutrinos coming from a source with known redshift z = 2, then we should find the flavor fraction given by the green star if the true value of H_0 is $H_0^{\rm LU}$. However, if the detected flavor-fraction is given by the green diamond, and we are certain about the source's redshift, then we deduce that $H_0 = H_0^{\rm EU}$.

Another observable that we can consider is the total neutrino flux. For a given flavor β, the total flux received at the detector, φ_{β_0}, is given by:

$$\begin{aligned}\varphi_{\beta_0} &= \sum_\alpha P_{\alpha\beta}\varphi_{\alpha_e} \\ &= \varphi_{\beta_e} + \sum_{\alpha;i<j}\left[a_{\alpha\beta;ij}\sin^2\left(\frac{\Delta m^2_{ij}\Delta\lambda}{4}\right) + b_{\alpha\beta;ij}\sin\left(\frac{\Delta m^2_{ij}\Delta\lambda}{2}\right)\right]\varphi_{\alpha_e}\end{aligned} \tag{14}$$

where Eq. (12) has been used in the second line and φ_{α_e} is the flux at emission. When analyzing astrophysical neutrino fluxes, it is usually assumed that it takes an empirical form $\varphi_{\alpha_e} \sim AE_\nu^{-\gamma}$, where A is a normalization constant and γ is the spectral index, for any flavor [40–42]. Therefore, the φ_{α_e}s on the right hand side (r.h.s) of Eq. (14) can be factorized, allowing us to form a fractional difference,

$$\delta\varphi_{\nu\beta} = \frac{\varphi_{\beta_0} - \varphi_{\beta_e}}{\varphi_{\beta_e}}, \tag{15}$$

[2] On the other hand, there is a clear distinction between the two for ND initial conditions. The fact that there is very little change for ND in the LU case is a distinctive feature compared to the other cases.

Table 1
Neutrino oscillation parameters used in the analysis as reported in [32].

Parameter	Normal Hierarchy (NH)	Inverted Hierarchy (IH)
$\sin^2(\theta_{12})$	0.307 ± 0.013	0.307 ± 0.013
Δm^2_{21}	$(7.53 \pm 0.18) \times 10^{-5}$ eV^2	$(7.53 \pm 0.18) \times 10^{-5}$ eV^2
$\sin^2(\theta_{13})$	$(2.18 \pm 0.07) \times 10^{-2}$	$(2.18 \pm 0.07) \times 10^{-2}$
$\sin^2(\theta_{23})$	0.545 ± 0.021	0.547 ± 0.021
Δm^2_{32}	2.453×10^{-3} eV^2	-2.546×10^{-3} eV^2
δ	$1.36 \pm 0.36\pi$ rad(2σ)	$1.36 \pm 0.36\pi$ rad(2σ)

between the observed and emitted fluxes, Fig. 2. Note that in these plots, the total flux for each flavor is being presented, i.e. summing over all ICs Eq. (13).

Let us now make a few comments about these plots. First, all diagrams of Fig. 2 show noticeable differences between hierarchies and EU/ LU values of H_0. To see this more clearly, we plot in Fig. 3 the fractional difference between EU and LU for each of the quantities appearing in Fig. 2 and for both hierarchies. That is, we look at

$$\delta\varphi_\alpha^{\rm EU-LU} = \frac{\varphi_{\alpha_0}^{\rm EU} - \varphi_{\alpha_0}^{\rm LU}}{\rm Max[\varphi_{\alpha_0}^{\rm EU}, \varphi_{\alpha_0}^{\rm LU}]} \tag{16}$$

for each hierarchy and flavor α, as a function of redshift. Even at relatively small redshifts ($z_e \sim 0.1$), using $H_0^{\rm EU}$ or $H_0^{\rm LU}$ makes a difference of a few % on the flux received.

Second, the starting values of Fig. 2's diagrams is related to the fact that our ICs, Eq. (13), are mainly of ν_e and ν_μ type. As they evolve with redshift, neutrinos start changing flavor to one another. In particular, ν_e and ν_μ are mostly transitioning to ν_τ, explaining the negative values of the top diagrams in Fig. 2. Moreover, there is a $\nu_\mu \to \nu_\tau$ transition as well, which can be seen from the decreasing (increasing) character of the middle (bottom) diagram in the aforementioned figure. However, since we started with more ν_μ than ν_e, in addition to $\nu_{e,\mu} \to \nu_\mu$ being more dominant than the other transitions, then we have $\varphi_{\mu_0} > \varphi_{\mu_e}$.

To give a more complete picture of how the difference between $H_0^{\rm EU}$ and $H_0^{\rm LU}$ affects neutrino oscillations, we can also look at the evolution of individual transition probabilities with redshift, as was done in [14]. However, in order to avoid clustering of diagrams, we report those in a GitHub repository [38].

4. Current and future observational prospects

Having laid down the theoretical part and its predictions, let us now discuss the observational prospects of detecting the distinctions presented in Figs. 1 and 2. When considering astrophysical neutrinos, especially extra-galactic ones, the most relevant neutrino observatory currently available is IceCube [36]. Therefore, in this section, we will focus on its potential detection of the effects we describe, be it with IceCube's current or future properties, IceCube-Gen2 [37].

Before doing that, let us briefly comment on the effect of Ω_m's uncertainty on the analysis above. As we are within the ΛCDM paradigm, spatial flatness is part of the model. This means that $\Omega_m + \Omega_\Lambda = 1$, and therefore there will be an uncertainty from Ω_m alone.[3] To test the effect of this uncertainty on our results, we varied the value of Ω_m within its error range given by the

[3] Note that solutions to the Hubble tension might induce additional uncertainties depending on their dynamics. However, as early-universe solutions to the tension are highly more favored than late-universe ones [12], the former will not affect neutrino observations relevant for IceCube and IceCube-Gen2. Therefore we do not expect further uncertainties to what we discuss above.

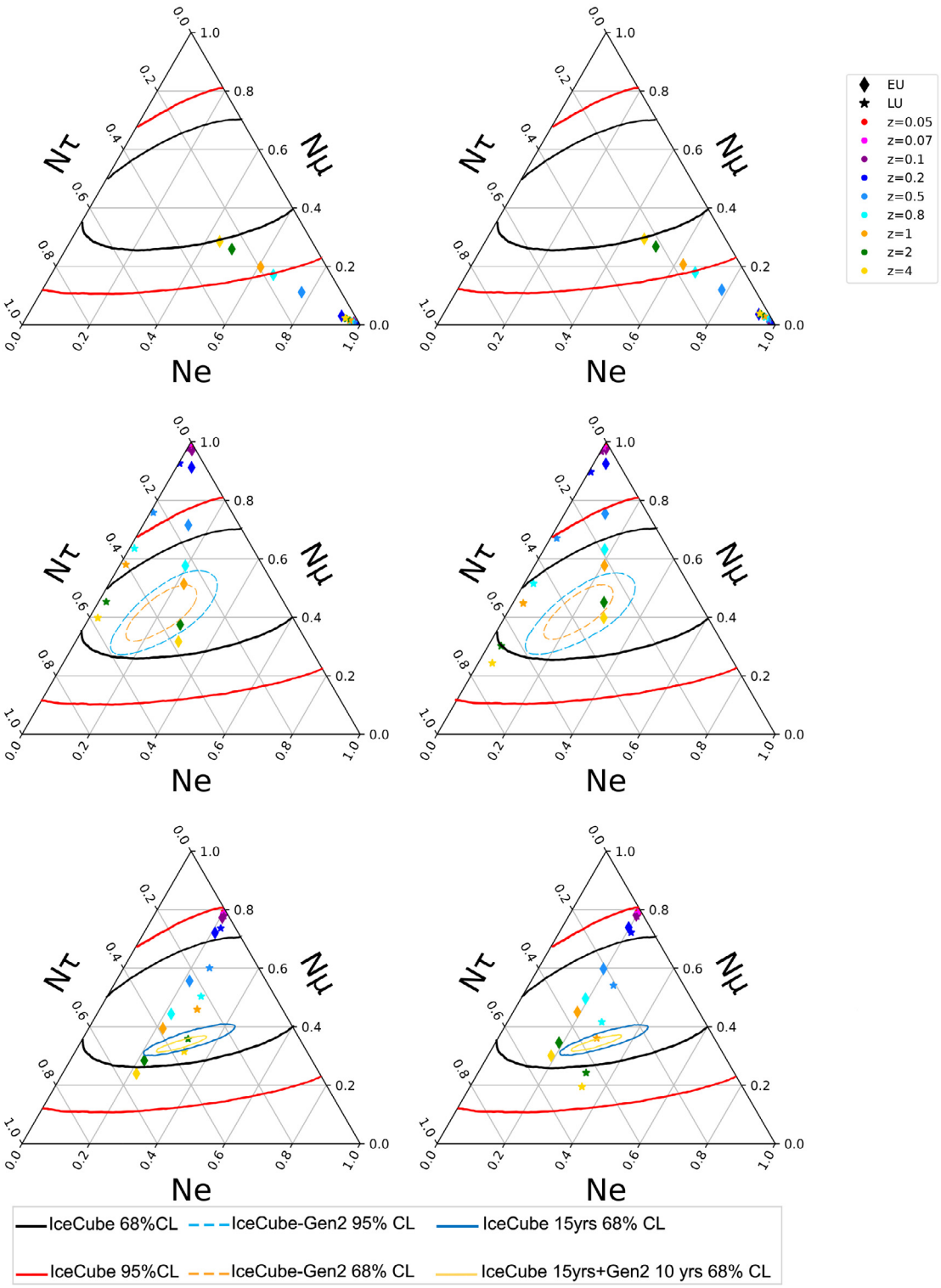

Fig. 1. Ternary plots of ND (top), MD (middle) and PD (bottom) initial neutrino flavor composition, Eq. (13), for NH (left) and IH (right). Diamond shaped points correspond to having H_0^{EU} as today's rate of expansion, while star shaped ones for H_0^{LU}. Different colors correspond to emission redshifts, as given by the legend above. We also include in every diagram the 95% and 68% Confidence Levels (CL) from IceCube, as presented in figure 5 of [37]. For the MD case, expected 68% (dashed orange) and 95% (dashed blue) CLs of IceCube-Gen2 are also shown (figure 17 of [37]). Finally, forecasts for 68%CL from 15 years of IceCube data(yellow contour) and that combined with 10 years of IceCube-Gen2 data (dark-blue contour) are shown for PD ICs (figure 20 of [37]). The python script to produce these is available in [38], which was written using [39]. (For interpretation of the references to color in this figure legend, the reader is referred to the web version of this article.)

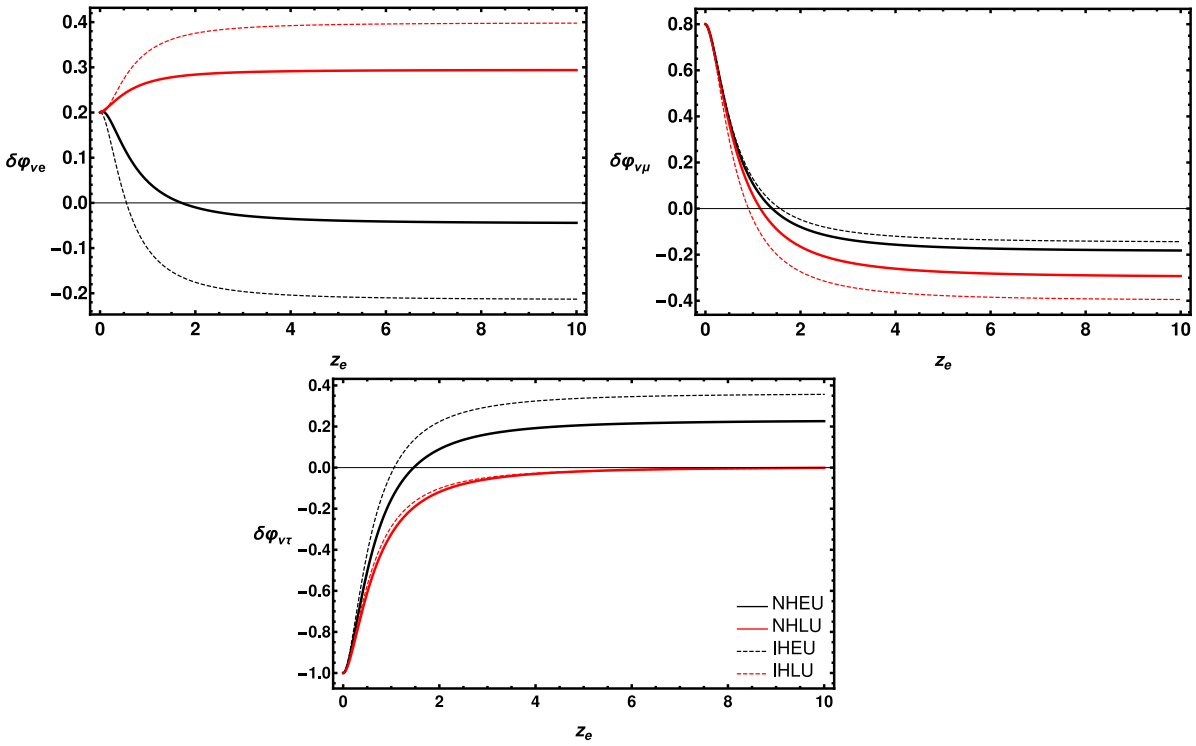

Fig. 2. Fractional difference, Eq. (15), between observed and emitted neutrino fluxes as a function of redshift. The presented $\delta\varphi$s are for ν_e (top-left), ν_μ (top-right) and ν_τ (bottom). Black curves correspond to having $H_0^{\rm EU}$, while red ones to $H_0^{\rm LU}$. On the other hand, solid lines refer to NH, while dashed ones to IH. The `Mathematica` script used to produce these is available in [38].

Planck-2018 data [3]. The result is that the integral in Eq. (11), which is the one that encompasses the effect we are studying, changes by only 0.12%. This change is expected when one uses propagation of error [43] to analyze the effect of this uncertainty on the results.

4.1. Prospects on flavor decomposition

In Fig. 1, we have included the latest 68% (black) and 95% (red) CLs from IceCube. These contours represent IceCube's observational constraints on neutrino flavor decomposition from a diffuse flux of neutrinos(i.e. from all directions in the sky). Nevertheless, these detected neutrinos eventually come from a certain source with a certain initial composition. Therefore, we can use these contours to constrain effects on neutrino flavors as they travel towards the detector.

In particular, from the top diagrams of Fig. 1, we can exclude the contribution of ND at the source traveling in a universe where $H_0 = H_0^{\rm LU}$ with more than 95% confidence. From the other diagrams in that figure, we can see that the most probable contribution to detected neutrinos comes from a PD rather than an MD initial composition. However, for the purpose of distinguishing between $H_0^{\rm LU}$ and $H_0^{\rm EU}$, current IceCube constraints cannot give much input.

On the other hand, IceCube-Gen2 will provide better prospects. As pointed out in [37], the upgraded detector will have 10 times more annual cosmic neutrino events, since it will be able to detect more promising neutrino sources that are 5 times fainter than the current ones (see Figs. 8–10 from [37]). For instance, from the contours in the middle diagrams of Fig. 1, we can see that the expected CLs from IceCube-Gen2 are leaning towards $H_0^{\rm EU}$ for the MD case. On the other hand, current forecasts for PD case are not as conclusive, as can be seen from the contours of the bottom diagrams in Fig. 1. However, we would like to stress that these expectations were calculated assuming the standard neutrino oscillations, i.e. assuming Minkowski spacetime. Once the accelerated expansion of spacetime is included in the analysis, these contours will differ, and then one can make proper conclusions about which value of H_0 is measured with neutrino observations. We will leave this subject for future work.

Before discussing the fluxes, it is worth emphasizing that having all the detected events to correspond to a particular IC is not necessary to make distinction between $H_0^{\rm EU}$ and $H_0^{\rm LU}$. Let us take, for instance, the particular case of ND ICs. Indeed, having 100% of detected neutrino sources to be from ND is not quite realistic. However, the measured diffuse neutrino flux is, in principle, a collection of many individual ones, each coming from a certain direction with its own flavor composition. As one can see from Fig. 1, the different ICs do not have degeneracy in their detection composition. Therefore, the latter allows one to identify which, out of the many detected fluxes, corresponds to ND. Such a scenario is indeed plausible, and is usually considered when analyzing neutrino data [37,44]. From here, one can then compare with the top diagrams of Fig. 1 to differentiate between values of H_0 without having 100% of the neutrino sources correspond to ND.

4.2. Prospects on neutrino fluxes

As briefly mentioned in the previous section, the measured and emitted neutrino fluxes have a power law form: $\phi \propto E_\nu^{-\gamma}$, where E_ν is the neutrino energy, and γ is the spectral index [45,46]. The fact that they have the same energy dependence can be seen from Eq. (14): since the expressions for the transition probabilities are known, then the observed flux must have the same form as the emitted one. Further, this consideration is corroborated by gamma-ray observations, from which one can deduce the emitted neutrino flux (see chapter 5 of [47]). Moreover, as previously mentioned, when analyzing neutrino observations, it is always assumed that they are traveling in a flat spacetime.

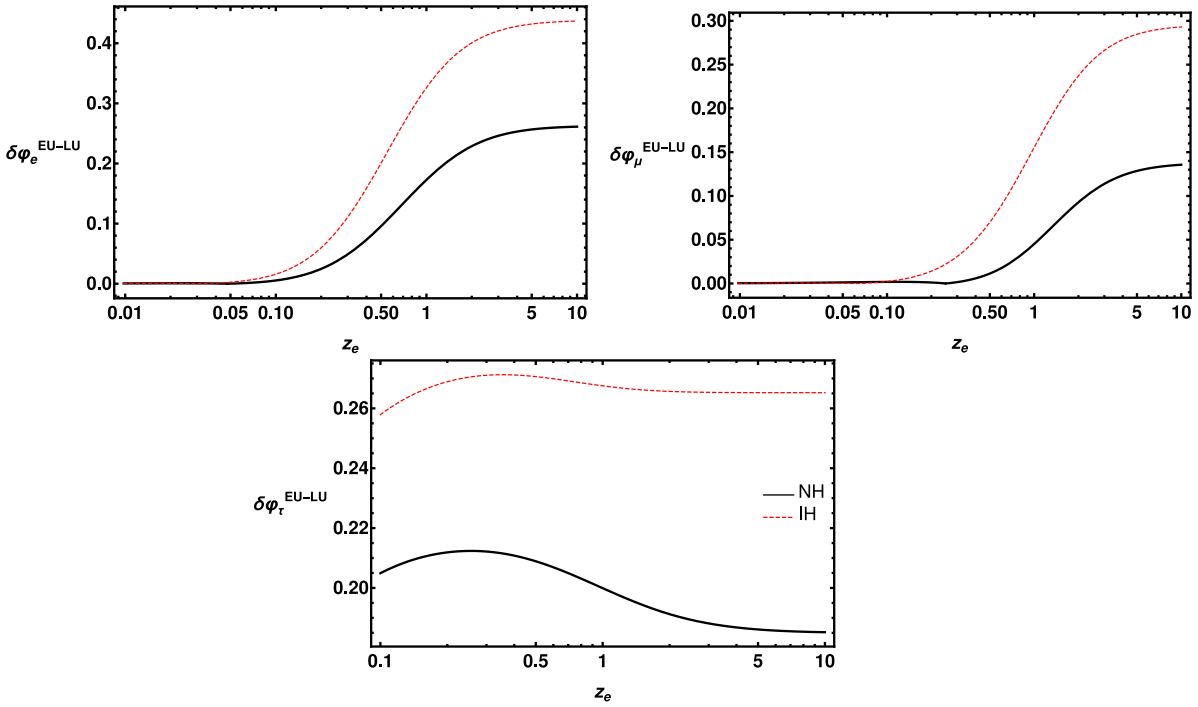

Fig. 3. Log-Linear plots of the fractional difference between EU and LU for each flavor flux as given in Eq. (16). The differences presented in each plot are for both hierarchies and correspond to ν_e (top-left), ν_μ (top-right) and ν_τ (bottom). The black-solid line correspond to having NH, while the red-dashed one to IH. The `Mathematica` script used to produce these is available in [38].

However, what we are pointing out in this work is that there could be up to 20% difference between the emitted and observed fluxes due to the accelerated expansion of the Universe.

It should be emphasized, however, that at the moment the measurement of fluxes form point sources has not been done with sufficiently high accuracy. Recently, IceCube has detected a few potential point sources, and the most promising ones to study the effect we are considering here are blazar TXS 0506+056 and GB6 J1542+6129 [48]. These two are situated at redshifts 0.33 and 0.5, respectively. However, there is still an uncertainty about these sources with current IceCube sensitivity, since they have been confirmed at 3.6σ and 2.9σ, respectively.

Nevertheless, there will be a significant improvement on this type of detection with IceCube-Gen2. As already pointed out, IceCube-Gen2's improved sensitivity will allow the detection of fainter possible sources of neutrinos, in addition to improvement on their flux measurements (see Figs. 8–10 from [37]).

Another important factor to this discussion, relevant for both flavor and flux measurements, is determining the redshift of a neutrino source. This determination mainly depends on the availability of a gamma-ray counterpart from that source. This was the case for the sources reported in [48]. Once that is the case, then one can do spectroscopic studies to determine the source's redshift, as has been done for TXS 0506+056 [49] and GB6 J1542+6129 [50], the most relevant sources for the case at hand. With IceCube-Gen2's increased sensitivity, and given that most of the additional sources will have a gamma-ray counterpart, then determining the redshift of the source is manageable in most of the cases.

5. Conclusion

With the persistence of a tension between early and late universe probes of today's expansion rate, H_0, using additional probes could shed some new light on the matter. In this work, which is an extension of previous ones [13,14], we demonstrated how neutrino oscillations can be such a probe.

We considered a system of three-flavors neutrinos as spinors in a flat FRW universe, with a cosmological constant DE, Λ. We use neutrino parameters, Table 1, and initial conditions, Eq. (13), to study the evolution of transition probabilities and neutrino fluxes with redshift. In particular, for each IC, Fig. 1 shows the detected flavor composition, distinguishing between H_0^{EU} and H_0^{LU} on the one hand, and between hierarchies on the other. Moreover, this distinction is presented for several redshifts of emission, demonstrating how the probability evolves with it. We can conclude from this that using H_0^{EU} or H_0^{LU} creates a difference of about 10% on neutrino oscillations, starting from a redshift of emission of about 0.2.

Concerning detection of neutrino fluxes, we consider the sum of all initial conditions in Eq. (13) for each neutrino flavor ν_e, ν_μ and ν_τ. Fractional difference between detected and emitted fluxes is shown in Fig. 2, for the four different combinations of hierarchies and early/late universe values of H_0. On the other hand, the fractional difference of the latter's effect on the fluxes is presented in Fig. 3. The same conclusion previously reached applies here as well, showing the potential of using neutrino oscillations as a new probe of the Hubble tension.

Finally, we studied the current and future observational prospects for the effect being analyzed in this work in Section 4. Current constraints from IceCube on flavor composition can already exclude ND initial condition in a universe with $H_0 = H_0^{\text{LU}}$ at more than 95%CL. However, decisive conclusions cannot yet be made at the moment due to IceCube's sensitivity. Nevertheless, this will change with IceCube-Gen2, as its sensitivity will increase 5 times compared to IceCube, resulting in 10 times more yearly events. Therefore, as is the case for using Gravitational Waves to measure H_0 [51], future observational prospects will add more insight on the relevance of the suggested method to the H_0 tension.

It is worth emphasizing that the considerations of this work are a mere generalization of neutrino oscillation studies to curved spacetime. No new entity or force have been added, rather a simple combination of distinct, well established, phenomena: neutrino oscillations and the Universe's accelerated expansion. Therefore, such an effect must be observed at some point in neutrino observatories [36,37], if it was not already in disguise. If this effect is not detected, even with the increasing performance of neutrino observatories [52], then this could hint to new Physics in the neutrino or gravitational sectors.

CRediT authorship contribution statement

Ali Rida Khalifeh: Conceptualization, Methodology, Software (Mathematica & Python), Validation, Formal analysis, Investigation, Resources, Data curation, Writing – original draft, Writing – review & editing, Visualization, Supervision, Project administration, Funding acquisition. **Raul Jimenez:** Software (Mathematica & Python), Validation, Formal analysis, Investigation, Visualization, Funding acquisition.

Declaration of competing interest

The authors declare that they have no known competing financial interests or personal relationships that could have appeared to influence the work reported in this paper.

Acknowledgments

We would like to thank Jordi Salvadó and Samuel Brieden from ICCUB and Claudio Kopper from the IceCube collaboration for extremely insightful discussions. The work of ARK and RJ is supported by MINECO grant PGC2018-098866-B-I00 FEDER, UE. ARK and RJ acknowledge "Center of Excellence Maria de Maeztu 2020-2023" award to the ICCUB (CEX2019- 000918-M).

References

[1] A.G. Riess, et al., A 2.4% determination of the local value of the Hubble constant, Astrophys. J. 826 (1) (2016) 56, http://dx.doi.org/10.3847/0004-637X/826/1/56, arXiv:1604.01424.

[2] L. Verde, T. Treu, A.G. Riess, Tensions between the early and late universe, Nature Astron. 3 (2019) 891–895, http://dx.doi.org/10.1038/s41550-019-0902-0, arXiv:1907.10625.

[3] N. Aghanim, et al., Planck Collaboration, Planck 2018 results. VI. Cosmological parameters, Astron. Astrophys. 641 (2020) A6, http://dx.doi.org/10.1051/0004-6361/201833910, arXiv:1807.06209.

[4] T.M.C. Abbott, et al., DES Collaboration, Dark energy survey year 3 results: Cosmological constraints from galaxy clustering and weak lensing, 2021, arXiv:2105.13549.

[5] N. Jackson, The Hubble constant, section 3, Living Rev. Rel. 10 (2007) 4, http://dx.doi.org/10.12942/lrr-2007-4, arXiv:0709.3924.

[6] M. Rowan-Robinson, Cosmological Distance Ladder: Distance and Time in the Universe, W.H.Freeman & Co, New York, NY (USA).

[7] A.G. Riess, et al., Observational evidence from supernovae for an accelerating universe and a cosmological constant, Astron. J. 116 (1998) 1009–1038, http://dx.doi.org/10.1086/300499, arXiv:astro-ph/9805201.

[8] K.C. Wong, et al., H0LiCOW – XIII. A 2.4 per cent measurement of H0 from lensed quasars: 5.3σ tension between early- and late-Universe probes, Mon. Not. R. Astron. Soc. 498 (1) (2020) 1420–1439, http://dx.doi.org/10.1093/mnras/stz3094, arXiv:1907.04869.

[9] T. Karwal, M. Kamionkowski, Dark energy at early times, the Hubble parameter, and the string axiverse, Phys. Rev. D 94 (10) (2016) 103523, http://dx.doi.org/10.1103/PhysRevD.94.103523, arXiv:1608.01309.

[10] F. Niedermann, M.S. Sloth, Resolving the Hubble tension with new early dark energy, Phys. Rev. D 102 (6) (2020) 063527, http://dx.doi.org/10.1103/PhysRevD.102.063527, arXiv:2006.06686.

[11] M. Ballardini, M. Braglia, F. Finelli, D. Paoletti, A.A. Starobinsky, C. Umiltà, Scalar-tensor theories of gravity, neutrino physics, and the H_0 tension, J. Cosmol. Astropart. Phys. 10 (2020) 044, http://dx.doi.org/10.1088/1475-7516/2020/10/044, arXiv:2004.14349.

[12] N. Schöneberg, G. Franco Abellán, A. Pérez Sánchez, S.J. Witte, V. Poulin, J. Lesgourgues, The H_0 Olympics: A fair ranking of proposed models, 2021, arXiv:2107.10291.

[13] A.R. Khalifeh, R. Jimenez, Spinors and scalars in curved spacetime: Neutrino dark energy (DE_ν), Phys. Dark Univ. 31 (2021) 100777, http://dx.doi.org/10.1016/j.dark.2021.100777, arXiv:2010.08181.

[14] A.R. Khalifeh, R. Jimenez, Distinguishing dark energy models with neutrino oscillations, Phys. Dark Univ. 34 (2021) 100897, http://dx.doi.org/10.1016/j.dark.2021.100897, arXiv:2105.07973.

[15] M. Escudero, S.J. Witte, A CMB search for the neutrino mass mechanism and its relation to the hubble tension, Eur. Phys. J. C 80 (4) (2020) 294, http://dx.doi.org/10.1140/epjc/s10052-020-7854-5, arXiv:1909.04044.

[16] M. Blasone, P. Jizba, L. Smaldone, Flavor energy uncertainty relations for neutrino oscillations in quantum field theory, Phys. Rev. D 99 (1) (2019) 016014, http://dx.doi.org/10.1103/PhysRevD.99.016014, arXiv:1810.01648.

[17] M. Blasone, G. Lambiase, G.G. Luciano, L. Petruzziello, L. Smaldone, Time-energy uncertainty relation for neutrino oscillations in curved spacetime, Classical Quantum Gravity 37 (15) (2020) 155004, http://dx.doi.org/10.1088/1361-6382/ab995c, arXiv:1904.05261.

[18] L. Buoninfante, G.G. Luciano, L. Petruzziello, L. Smaldone, Neutrino oscillations in extended theories of gravity, Phys. Rev. D 101 (2) (2020) 024016, http://dx.doi.org/10.1103/PhysRevD.101.024016, arXiv:1906.03131.

[19] A. Capolupo, G. Lambiase, A. Quaranta, Neutrinos in curved spacetime: Particle mixing and flavor oscillations, Phys. Rev. D 101 (2020) 095022, http://dx.doi.org/10.1103/PhysRevD.101.095022, URL https://link.aps.org/doi/10.1103/PhysRevD.101.095022.

[20] C.Y. Cardall, G.M. Fuller, Neutrino oscillations in curved spacetime: A heuristic treatment, Phys. Rev. D 55 (1997) 7960–7966, http://dx.doi.org/10.1103/PhysRevD.55.7960, URL https://link.aps.org/doi/10.1103/PhysRevD.55.7960.

[21] D.B. Kaplan, A.E. Nelson, N. Weiner, Neutrino oscillations as a probe of dark energy, Phys. Rev. Lett. 93 (2004) 091801, http://dx.doi.org/10.1103/PhysRevLett.93.091801, URL https://link.aps.org/doi/10.1103/PhysRevLett.93.091801.

[22] S. Ando, M. Kamionkowski, I. Mocioiu, Neutrino oscillations, Lorentz/*CPT* violation, and dark energy, Phys. Rev. D 80 (2009) 123522, http://dx.doi.org/10.1103/PhysRevD.80.123522, URL https://link.aps.org/doi/10.1103/PhysRevD.80.123522.

[23] N. Klop, S. Ando, Effects of a neutrino-dark energy coupling on oscillations of high-energy neutrinos, Phys. Rev. D 97 (2018) 063006, http://dx.doi.org/10.1103/PhysRevD.97.063006, URL https://link.aps.org/doi/10.1103/PhysRevD.97.063006.

[24] H. Mohseni Sadjadi, H. Yazdani Ahmadabadi, Damped neutrino oscillations in a conformal coupling model, Phys. Rev. D 103 (2021) 065012, http://dx.doi.org/10.1103/PhysRevD.103.065012, URL https://link.aps.org/doi/10.1103/PhysRevD.103.065012.

[25] H. Mohseni Sadjadi, A.P. Khosravi, Symmetry breaking, and the effect of matter density on neutrino oscillation, J. Cosmol. Astropart. Phys. 04 (2018) 008, http://dx.doi.org/10.1088/1475-7516/2018/04/008, arXiv:1711.06607.

[26] G.G. Luciano, M. Blasone, Gravitational effects on neutrino decoherence in the lense–thirring metric, Universe 7 (11) (2021) 417, http://dx.doi.org/10.3390/universe7110417, arXiv:2110.00971.

[27] A.G. Riess, S. Casertano, W. Yuan, L.M. Macri, D. Scolnic, Large magellanic cloud cepheid standards provide a 1% foundation for the determination of the Hubble constant and stronger evidence for physics beyond ΛCDM, Astrophys. J. 876 (1) (2019) 85, http://dx.doi.org/10.3847/1538-4357/ab1422, arXiv:1903.07603.

[28] S. Dodelson, F. Schmidt, Modern Cosmology, second ed., Academic Press, 2020.

[29] O.F. Piattella, Lecture Notes in Cosmology, in: UNITEXT for Physics, Springer, Cham, 2018, http://dx.doi.org/10.1007/978-3-319-95570-4, arXiv:1803.00070.

[30] B. Pontecorvo, Neutrino experiments and the problem of conservation of leptonic charge, Zh. Eksp. Teor. Fiz. 53 (1967) 1717–1725.

[31] Z. Maki, M. Nakagawa, S. Sakata, Remarks on the unified model of elementary particles, Progr. Theoret. Phys. 28 (5) (1962) 870–880, http://dx.doi.org/10.1143/PTP.28.870, arXiv:https://academic.oup.com/ptp/article-pdf/28/5/870/5258750/28-5-870.pdf.

[32] P.D. Group, Review of particle physics, chapter 14.3, Prog. Theor. Exp. Phys. 2020 (8) (2020) 083C01, http://dx.doi.org/10.1093/ptep/ptaa104, arXiv:https://academic.oup.com/ptep/article-pdf/2020/8/083C01/34673722/ptaa104.pdf.

[33] H. Nunokawa, S.J. Parke, J.W.F. Valle, CP violation and neutrino oscillations, Prog. Part. Nucl. Phys. 60 (2008) 338–402, http://dx.doi.org/10.1016/j.ppnp.2007.10.001, arXiv:0710.0554.

[34] A. Baha Balantekin, B. Kayser, On the properties of neutrinos, Ann. Rev. Nucl. Part. Sci. 68 (2018) 313–338, http://dx.doi.org/10.1146/annurev-nucl-101916-123044, arXiv:1805.00922.
[35] C. Giunti, C.W. Kim, Fundamentals of Neutrino Physics and Astrophysics, Chapter 13.1, Oxford University Press, 2007.
[36] IceCube Collaboration, The detection of a sn iin in optical follow-up observations of icecube neutrino events, Astrophys. J. 811 (1) (2015) 52, http://dx.doi.org/10.1088/0004-637x/811/1/52.
[37] M.G. Aartsen, et al., IceCube-Gen2 Collaboration, IceCube-Gen2: The window to the extreme universe, J. Phys. G 48 (6) (2021) 060501, http://dx.doi.org/10.1088/1361-6471/abbd48, arXiv:2008.04323.
[38] A.R. Khalifeh, NeutrinoOscillation-H0Tension, 2021, http://dx.doi.org/10.5281/zenodo.1234, URL https://github.com/ark93-cosmo/NeutrinoOscillation-H0Tension.
[39] Y. Ikeda, B. Grabowski, F. Körmann, mpltern 0.3.0: Ternary Plots as Projections of Matplotlib, Zenodo, 2019, http://dx.doi.org/10.5281/zenodo.3528355.
[40] R. Abbasi, et al., IceCube Collaboration, The IceCube high-energy starting event sample: Description and flux characterization with 7.5 years of data, Phys. Rev. D 104 (2021) 022002, http://dx.doi.org/10.1103/PhysRevD.104.022002, arXiv:2011.03545.
[41] M.G. Aartsen, et al., IceCube Collaboration, Evidence for astrophysical muon neutrinos from the northern sky with IceCube, Phys. Rev. Lett. 115 (2015) 081102, http://dx.doi.org/10.1103/PhysRevLett.115.081102, URL https://link.aps.org/doi/10.1103/PhysRevLett.115.081102.
[42] C.A. Argüelles, K. Farrag, T. Katori, R. Khandelwal, S. Mandalia, J. Salvado, Sterile neutrinos in astrophysical neutrino flavor, J. Cosmol. Astropart. Phys. 02 (2020) 015, http://dx.doi.org/10.1088/1475-7516/2020/02/015, arXiv:1909.05341.
[43] J.R. Taylor, An Introduction To Error Analysis: The Study of Uncertainties in Physical Measurements, Chapter 3, University Science Books, 55D Gate Five Road Sausalito, CA 94965, 1997.
[44] A. Palladino, The flavor composition of astrophysical neutrinos after 8 years of IceCube: an indication of neutron decay scenario? Eur. Phys. J. C 79 (6) (2019) 500, http://dx.doi.org/10.1140/epjc/s10052-019-7018-7, arXiv:1902.08630.
[45] J. Stettner, IceCube Collaboration, Measurement of the diffuse astrophysical muon-neutrino spectrum with ten years of IceCube data, PoS ICRC 2019 (2020) 1017, http://dx.doi.org/10.22323/1.358.1017, arXiv:1908.09551.
[46] R. Abbasi, et al., IceCube Collaboration, Measurement of astrophysical tau neutrinos in IceCube's high-energy starting events, 2020, arXiv:2011.03561.
[47] F. Halzen, A. Kheirandish, IceCube and high-energy cosmic neutrinos, 2022, arXiv:2202.00694.
[48] M.G. Aartsen, et al., Time-integrated neutrino source searches with 10 years of IceCube data, Phys. Rev. Lett. 124 (2020) 051103, http://dx.doi.org/10.1103/PhysRevLett.124.051103, URL https://link.aps.org/doi/10.1103/PhysRevLett.124.051103.
[49] S. Paiano, R. Falomo, A. Treves, R. Scarpa, The redshift of the BL Lac object TXS 0506+056, Astrophys. J. Lett. 854 (2) (2018) L32, http://dx.doi.org/10.3847/2041-8213/aaad5e, arXiv:1802.01939.
[50] M.J.M. Marcha, A. Caccianiga, The CLASS BL Lac sample: The radio luminosity function, Mon. Not. R. Astron. Soc. 430 (2013) 2464, http://dx.doi.org/10.1093/mnras/stt065, arXiv:1301.6550.
[51] B.P. Abbott, et al., LIGO Scientific, Virgo, 1M2H, Dark Energy Camera GW-E, DES, DLT40, Las Cumbres Observatory, VINROUGE, MASTER Collaboration, A gravitational-wave standard siren measurement of the Hubble constant, Nature 551 (7678) (2017) 85–88, http://dx.doi.org/10.1038/nature24471, arXiv:1710.05835.
[52] S. Böser, M. Kowalski, L. Schulte, N.L. Strotjohann, M. Voge, Detecting extra-galactic supernova neutrinos in the Antarctic ice, Astropart. Phys. 62 (2015) 54–65, http://dx.doi.org/10.1016/j.astropartphys.2014.07.010, arXiv:1304.2553.